Retrieval of Surface and Atmospheric Geophysical Variables over Snow-Covered Land from Combined Microwave and Infrared Satellite Observations

C. PRIGENT

CNRS, LERMA, Observatoire de Paris, Paris, France

F. AIRES

Department of Applied Physics, Columbia University, NASA Goddard Institute for Space Studies, New York, New York

W. B. ROSSOW

NASA Goddard Institute for Space Studies, New York, New York

(Manuscript received 20 May 2002, in final form 18 September 2002)

ABSTRACT

Surface temperature and emissivities, as well as atmospheric water vapor and cloud liquid water, have been calculated from Special Sensor Microwave Imager observations for snow-covered land areas using a neural network inversion scheme that includes first-guess information. A learning database to train the neural network is derived from a global collection of coincident surface and atmospheric parameters, extracted from the National Centers for Environmental Prediction reanalysis, from the International Satellite Cloud Climatology Project data, and from microwave emissivity atlases previously calculated. Despite the large space and time variability of the snow microwave response, the surface and atmospheric parameters are retrieved. Water vapor is estimated with a theoretical rms error of approximately 30%, verified against radiosonde measurements, that is almost the same as over snow-free land. The theoretical rms error of the surface skin temperature retrieval is 1.5 and 1.9 K, respectively, for clear and cloudy scenes. The surface skin temperatures are compared with the surface air temperatures measured at meteorological stations to verify that the expected differences are found. The space and time variations of the retrieved surface emissivities are evaluated by comparison with surface parameter variations such as surface air temperature, snow depth, and vegetation cover.

1. Introduction

The mean monthly land area covered by snow in the Northern Hemisphere ranges from ~10% to ~40% during the annual cycle. Because of its high albedo, snow extent is a primary factor controlling the amount of solar radiation absorbed by the earth. Even a shallow snow cover can increase the albedo of a bare landscape from 0.2 to 0.8. Any decrease in snow cover related to a warming trend would result in increased absorption of solar radiation, melting the snow and inducing a positive feedback. As a consequence, the cryospheric components of the climate are regarded as sensitive indicators of changes. Snow cover also interacts with and modifies the overlying air masses, considerably influencing the atmospheric circulation, not only in polar regions but also at midlatitudes, making assimilation of observations in polar regions crucial for numerical weather prediction (NWP) models. In addition, snow is a dominant source of delayed water supply in the northern regions, with large impact on the global hydrological budget.

Conventional measurements in remote polar areas unfortunately are sparse, thus limiting the ability to monitor meteorological, hydrological, and climatological processes accurately in these regions. Satellite observations provide a unique opportunity to monitor continuously the whole polar region with great detail.

Passive microwave satellite observations over snow have been used to estimate snow cover and depth (e.g., Kunzi et al. 1982; Chang et al. 1987; Hall et al. 1991; Foster et al. 1996b; Grody and Basist 1996; Pulliainen and Hallikainen 2001), with the substantial advantages over visible observations that the microwave observations do not depend on the solar illumination, are not limited to cloud-free areas, and are sensitive to snow depth. However, global applications of snow-depth algorithms are questioned, and several studies have suggested the need for regionally specific adjustments (Foster et al. 1996a; Robinson and Spies 1994) or adding extra information in the retrieval process [e.g., land clas-

Corresponding author address: C. Prigent, CNRS, LERMA, Observatoire de Paris, 61, avenue de l'Observatoire, Paris 75014, France.
E-mail: catherine.prigent@obspm.fr

sification, topography, air temperature (Singh and Gan 2000), or temperature history (Josberger and Mognard 2002)]. In addition, when compared with visible or infrared observations, microwave observations have coarser spatial resolution, creating problems when interpreting heterogeneous footprints that cover mixtures of surface types and snow characteristics.

Retrieval of surface and atmospheric parameters over snow with passive microwave observations is a complex and ill-posed inverse problem. The surface responses are not only highly variable in space and time, they are also very difficult to model because they are sensitive to a variety of parameters, such as snow particle sizes, wetness, and potential embedded vegetation. The space and time variability of the snow emissivities is discussed in section 2, and a brief review of previous theoretical and experimental work helps to interpret the variability in terms of snow characteristics. A neural network inversion scheme has been developed to retrieve surface temperatures, surface emissivities, atmospheric water vapor, and cloud liquid water over snow- and ice-free land from the Special Sensor Microwave Imager (SSM/I) observations (Aires et al. 2001), using precalculated monthly mean emissivities and clear-sky infrared measurements of surface temperatures as first-guess information. This study explores the feasibility of using this technique over snow-covered surfaces. Major challenges are the larger space and time variability of the emissivities, modeling the possibility of volume scattering within the snowpack, and the problem of detection of low water vapor contents. Section 3 describes the neural network inversion method to retrieve simultaneously the surface temperature Ts, the seven surface emissivities e_f, the atmospheric water vapor WV, and the cloud liquid water path LWP over snow. The theoretical performance of the retrieval method is also presented. The neural network method is applied to a year of SSM/I data. Results are discussed and are compared with available in situ measurements (section 4). Section 5 concludes this study by highlighting the need for a thorough analysis of the variability of the snow emissivity with the physical characteristics of the snowpack.

2. Variability of microwave snow emissivities

A snowpack can consist of several layers having different densities and crystal-size distributions. The properties of these layers reflect the snowpack's history and relate to location and elevation. Sturm et al. (1995), for instance, suggest separating the snow into six classes: tundra, taiga, alpine, maritime, prairie, and ephemeral, each type having a unique ensemble of textural and stratigraphic characteristics, including the sequence of snow layers, their thickness, density, crystal morphology, and grain.

Microwave radiation responds to snowpack properties such as density, depth, crystal-size distribution, vertical temperature gradient, surface wetness, melting–refreezing cycles, and embedded or covering vegetation. The responses of microwave radiation to these surface characteristics are usually highly dependent on frequency. An extensive amount of research has been directed toward a better understanding of the mechanisms responsible for the microwave emission of snow, both modeling analysis and ground-based or aircraft experiments.

Modeled microwave emissivities of snow are particularly sensitive to snow water equivalent, grain size, and snow wetness. The dielectric losses in dry snow are very small, so the extinction coefficient is dominated by scattering, this effect being stronger at shorter wavelengths for larger particles and drier snow. The first numerical results for dry snow used conventional Mie scattering theory and predicted a steep decrease of the brightness temperatures with grain size, (e.g., Chang et al. 1976). Calculations using ''dense medium'' theory show that the scattering is less than predicted with the assumption of independent scattering used by the Mie scattering theory (e.g., Tsang 1992).

Large differences in the dielectric properties of liquid and frozen water at microwave frequencies produce substantial variations of the snow emissivity with wetness and melting. With increasing wetness, the dielectric losses become large and the scattering becomes negligible. Wet snowpacks radiate like blackbodies at the physical temperature of the upper snow layer. In the spring, snow undergoes melting and refreezing cycles during which large spherical grains are formed. Grain sizes can increase by a factor of 2–3 by the end of the winter (Sturm and Benson 1997). Thus, the microwave signature of the snowpack varies between blackbody behavior for wet snow to high reflectivities due to strong volume scattering by the large inhomogeneities. This effect is especially sensitive at higher frequencies.

Field experiments have been conducted to analyze the snow emissivity with respect to the characteristics of the snowpack. The University of Bern has been particularly active with ground-based measurements in the Alps (e.g., Schanda et al. 1983; Matzler 1994), and several aircraft measurement campaigns have been conducted in Finland by the University of Helsinki and by the U.K. Met Office (e.g., Kurvonen and Hallikainen 1997; Hewison and English 1999). Measurements confirm the large variability of the snow emissivities with snow characteristics and history. Matzler (1994) measures emissivities of various landscapes in winter between 5 and 100 GHz at 50° incidence and searches for specific microwave signatures that would enable unambiguous retrieval of snow parameters from microwave observations. He concludes that estimation of snow water equivalent is not feasible solely from passive microwave observations in this range. However, snow cover can be discriminated from other surfaces, even for fresh powder snow when using the higher frequencies.

Microwave emissivities over the globe have been estimated from SSM/I at 19.35, 22.235, 37.0, and 85.5

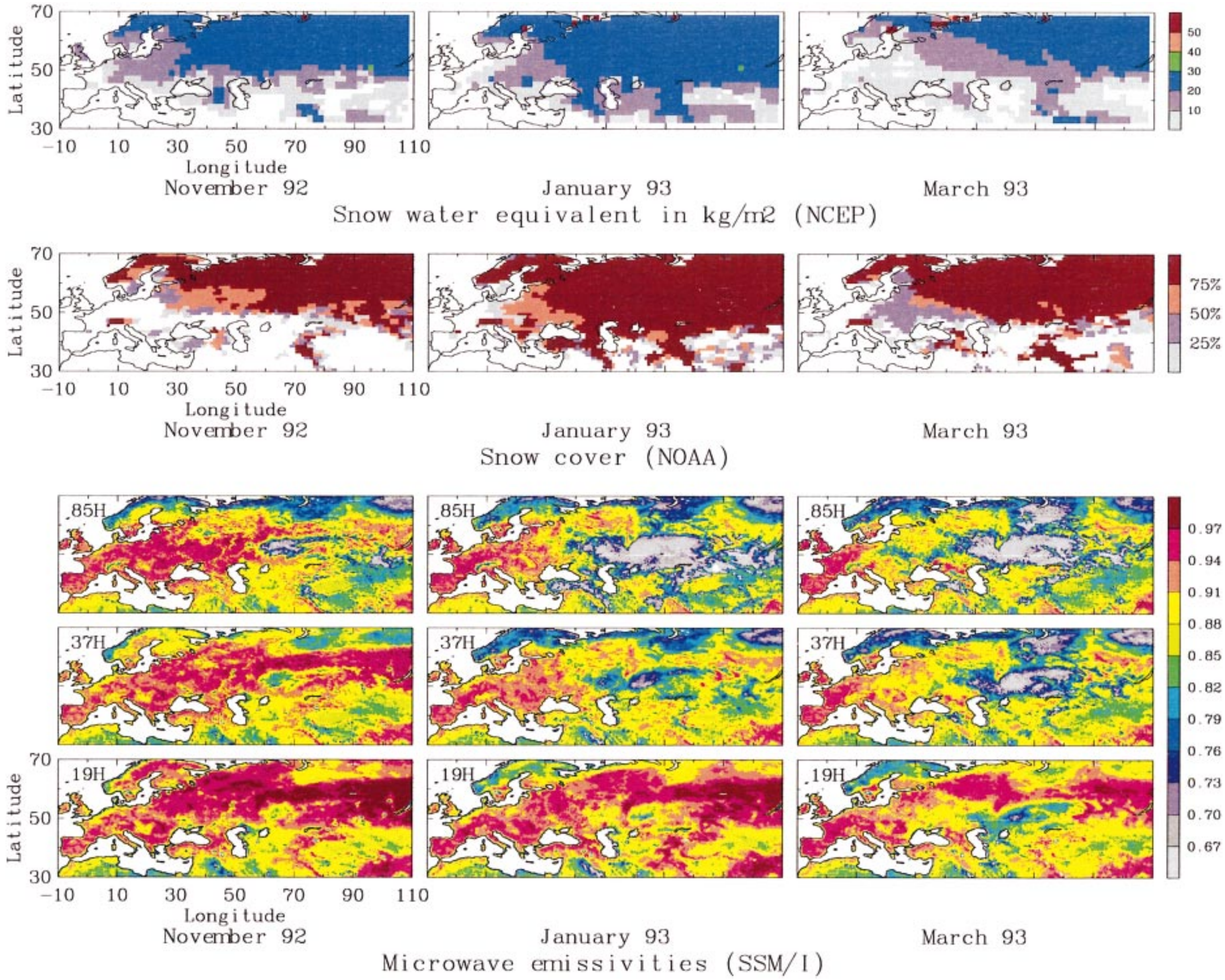

FIG. 1. Monthly mean effective emissivities at 19, 37, and 85 GHz for horizontal polarization for Nov 1992, Jan 1993, and Mar 1993. Also presented are the snow-cover information derived from the NOAA operational analysis and the monthly mean snow water equivalent extracted from the NCEP reanalysis.

GHz (Prigent et al. 1997, 1998) by removing the contributions of the atmosphere, clouds, and rain with the help of ancillary satellite data [International Satellite Cloud Climatology Project (ISCCP; Rossow and Schiffer 1991, 1999)] and meteorological reanalysis from the National Centers for Environmental Prediction (NCEP; Kalnay et al. 1996), and by using infrared surface skin temperature estimates from ISCCP. In the first step, cloud-free SSM/I observations are isolated with the help of collocated visible/infrared satellite observations (ISCCP data). The cloud-free atmospheric contribution is then calculated from an estimate of the local atmospheric temperature–humidity profile (NCEP reanalysis). Last, the surface emissivity is calculated for all of the SSM/I channels, for all cloud-free pixels, assuming that the reflection is specular and the microwave radiation emanates only from a thin surface layer. The surface temperature is thus the surface skin temperature estimated from the infrared measurements (derived from ISCCP), neglecting surface and volume scattering. The emissivities are ''effective'' emissivities calculated according to specular assumptions. Without prior information on the detailed characteristics of the snow cover, more accurate radiative transfer assumptions cannot be implemented on a global basis. These practical assumptions enable a consistent suppression of the atmospheric contributions and surface temperature modulations. Retrievals are performed on an equal-area grid equivalent to $0.25° \times 0.25°$ at the equator. For each pixel and each frequency, a monthly mean emissivity is calculated along with the standard deviation of the day-to-day emissivity variations within each month.

The retrieved monthly mean effective emissivities are displayed at 19, 37, and 85 GHz for horizontal polarization (Fig. 1) for November of 1992, January of 1993, and March of 1993. Also presented is the snow cover defined for each location as the number of fully snow covered pixels processed during the month divided by the total number of SSM/I pixels for that month at that location, the snow-cover information being derived from the National Oceanic and Atmospheric Administration (NOAA) operational analysis. The monthly mean snow water equivalent derived from the NCEP reanalysis is also shown in Fig. 1. For a given month and a given frequency, the most striking feature is the large variability of snow emissivities without noticeable variations in the snow cover derived from NOAA or in the snow water equivalent estimated by NCEP. The high sensitivity of the 85 GHz to the snow properties is exhibited by distinctive signatures over the Alps for the 3 months or over the Zagros Mountains (northwest of Iran, Armenia, and east of Turkey) in January and March, whereas the variations are much weaker at 37 GHz and are nonexistent at 19 GHz. The substantially different behaviors of the snow emissivities for these three frequencies can be explained by increasing scattering with increasing frequency for dry snow in cold mountainous environments. For a given area (north of Kazakstan or in Russia, east of the Ural Mountains, for instance), the emissivity decreases with time during the winter season. By the end of the winter, snow has undergone multiple thawing and refreezing cycles during which larger spherical grains are formed (Sturm and Benson 1997). The microwave signature of the snowpack then varies between characteristics for wet snow to higher reflectivities due to scattering by the large inhomogeneities. There is a sharp discontinuity parallel to the Ural Mountains in Russia, especially at 37 and 85 GHz: west of the Ural Mountains, the snow emissivities are high while they are much lower on the east side of the range. Vegetation density decreases from west to east of the Ural Mountains, with evergreen needle–leaved forest in the west and increasing coverage of deciduous forest and tundra eastward (Matthews 1983). In addition, the decreasing air temperature from west to east can also contribute to a different snow behavior, with possibly drier snow east of the mountain range. The emissivities for vertical polarization present similar highly variable features, with 19 GHz very weakly sensitive to the presence of snow and increasing scattering signatures with increasing frequency.

Figure 2 shows the normalized histograms of the standard deviations of the microwave emissivities calculated on a monthly basis at 19, 37, and 85 GHz for both polarizations, for snow-free land areas (solid lines) and for snow-covered land (dashed lines). As expected, the time variability of the microwave response over snow increases with frequency and is larger for horizontal polarization than for vertical polarization, especially at lower frequencies. Snow emissivity not only varies on a monthly timescale, it can also undergo changes on timescales as short as a day, with thawing and refreezing cycles induced by diurnal variations of air temperature.

Local measurements and modeling studies have shown the influence of snow characteristics, such as snow depth, wetness, or grain-size distributions, on the microwave responses. However, on a regional basis or over longer times, it is very difficult to show direct correlations between the snow properties and the microwave observations. First, the snow characteristics that influence the microwave responses are all variable in space and time and are intricately mixed with each other and with temperature variations, making it difficult to isolate and to analyze the effect of a single parameter alone. Second, most snow properties that are likely to affect the microwave responses are not routinely measured, making verifications of satellite retrievals very difficult.

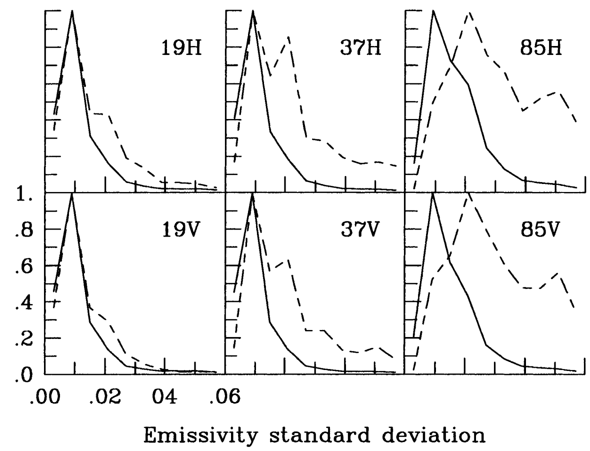

FIG. 2. Normalized histograms of the standard deviations of the microwave emissivities calculated on a monthly basis at 19, 37, and 85 GHz for both polarizations, for snow-free land areas (solid lines) and for snow-covered land (dashed lines).

The National Meterological Center (NMC, now NCEP) observational data include snow depth for a large number of stations in the United States and in Canada. This dataset has been obtained and analyzed for a year in coincidence with the microwave observations. Table 1 gives the linear correlation coefficients between the SSM/I brightness temperatures Tb and the snow depth for clear and cloudy scenes (the cloud flag comes from the ISCCP dataset). The correlation is always very low, even for the brightness temperature difference between 19 and 37 GHz, which is the basis for commonly used snow depth algorithms (e.g., Kunzi et al. 1982; Chang et al. 1987). The linear correlation coefficients have also been calculated for the surface skin temperature extracted from ISCCP for clear conditions (Table 1). It shows values up to about 0.7, much higher than the linear coefficients obtained with the snow depth. These correlations do not distinguish direct dependences between variables from indirect ones due to intermediate variables: variables that are not physically related can be statistically correlated via a third variable. These calculations assume linear relationships between

TABLE 1. Linear correlation coefficients calculated for Jan, Feb, and Mar 1993 over North America.

	Snow depth (in situ)	Surface skin temperature (ISCCP)
	Clear	
Tb_{19V}	−0.26	0.68
Tb_{19H}	−0.15	0.54
Tb_{22V}	−0.29	0.73
Tb_{37V}	−0.31	0.70
Tb_{37H}	−0.23	0.65
Tb_{85V}	−0.09	0.59
Tb_{85H}	−0.07	0.59
$Tb_{37V} - Tb_{19V}$	0.24	−0.45
$Tb_{37H} - Tb_{19H}$	0.21	−0.39
	Cloudy	
Tb_{19V}	−0.18	—
Tb_{19H}	−0.12	—
Tb_{22V}	−0.20	—
Tb_{37V}	−0.23	—
Tb_{37H}	−0.18	—
Tb_{85V}	−0.02	—
Tb_{85H}	−0.08	—
$Tb_{37V} - Tb_{19V}$	0.19	—
$Tb_{37H} - Tb_{19H}$	0.17	—

the variables, but nonlinear relationships are more likely.

In conclusion, the microwave response over snow is very variable in time and space, and its variations can not be easily attributed to a simple set of snowpack characteristics that are linearly correlated with the microwave signal. As already noticed by several authors (e.g., Foster et al. 1994; Matzler 1994), the SSM/I 85-GHz channels show an interesting sensitivity to the presence and depth of shallow snow or fresh dry powder snow. However, its use has been so far very limited over snow because of the water vapor and cloud contamination at this frequency. When using brightness temperatures directly, even in polar regions, the amount of atmospheric contamination is not negligible even at 37 GHz, especially in cloudy areas (Rott and Nagler 1994), and the effect increases with frequency. Abdalati and Steffen (1997) emphasize the impact of the atmospheric variability, especially during the melting season, in low-elevation areas where the water vapor and cloud contamination can be significant. In a preparatory study for the Multifrequency Imager Microwave Radiometer, Noll et al. (1994) also recommend combining retrievals of atmospheric and surface parameters at microwave frequencies to account for the effects of the atmospheric variability on the surface parameter retrieval.

The problem is thus to retrieve surface and atmospheric parameters over a highly variable surface, for atmospheres that contain low water vapor amount, given in addition that the surface and the atmospheric contributions are intricately mixed.

3. Retrieval method

A neural network inversion scheme, including first-guess information, has been developed to retrieve Ts, e_f, WV, and LWP over snow- and ice-free land from SSM/I (Aires et al. 2001). The current study explores the feasibility of this technique over snow-covered surfaces: a major problem being the higher space and time variability of the surface characteristics when compared with snow-free areas.

The neural network method optimizes the use of all the SSM/I channels and the prior information to constrain the inversion problem and retrieves simultaneously the surface and atmospheric parameters that are consistent among themselves and with the satellite observations. The neural network is designed by analyzing all of the local statistical relationships in the learning database and benefits from them, even when the relationships are highly nonlinear. These relationships represent nonlinear correlations among the physical variables, among the observations (brightness temperatures), among the first guesses, and between the variables and the observations. All of these correlations constitute additional information that the neural network can exploit to improve its retrieval if such nonlinear correlations are properly represented in the learning dataset. In contrast, the variational assimilation scheme, in its classical implementation, can only use the linear correlations between the variables. See Aires et al. (2001) for a comparison of the neural network and variational approaches.

a. Learning algorithm with first guess

The neural network scheme is briefly described. For more details see Aires et al. (2001). The multilayer perceptron (MLP) network is a nonlinear mapping model composed of distinct layers of neurons: the first layer S_0 represents the input $X = (x_i;\ i \in S_0)$ of the mapping; the last layer S_L represents the output mapping $Y = (y_k;\ k \in S_L)$; and the intermediate layers S_m $(0 < m < L)$ are called the hidden layers. These layers are connected via neural links. We denote the parameters of these links by W.

To avoid nonuniqueness and/or instability in an inverse problem, it is essential to use all preexisting information available: the chosen solution is then constrained so that it is physically more coherent. Introduction of a priori first-guess information into a neural network model was first proposed by Aires et al. (2001). With the prior information included in the input of the classical MLP network, the neural transfer function becomes

$$\hat{y} = g_W(y^b, x^o), \tag{1}$$

where $\hat{y}$ is the retrieval (i.e., retrieved physical parameters), g_W is the neural network with parameters W, y^b is the first guess for the retrieval of physical parameters y, and x^o is the noisy observations.

The error back-propagation algorithm (Rumelhart et al. 1986) is the learning algorithm that estimates the optimal network parameters W by minimizing a cost function $C(W)$, approaching as closely as possible the desired function (i.e., inverse of the radiative transfer equation). The criterion usually used to derive W is the mean-square errors in network outputs

$$C(W) = \frac{1}{2}\iiint D_E[g_w(y+\varepsilon, x+\eta), y]^2\, P(x)\, P_\eta(\eta)\, P_\varepsilon(\varepsilon), \tag{2}$$

where D_E is the Euclidean distance between $\hat{y} = g_W(y + \varepsilon, x + \eta)$, the network output, and y is the desired output. The distance D_E is implicitly here in the space of the physical parameters y (same dimension as S_L); $P(y)$ is the probability distribution function of the physical variables y that depends on their natural variability; $P_\eta(\eta)$ is the probability distribution function of the observation noise η; $P_\varepsilon(\varepsilon)$ is the probability distribution function of the first-guess error $\varepsilon = y^b - y$.

To minimize the criterion of Eq. (2), we create a learning database

$$\mathcal{B} = \{(y^e, x^{oe}, y^{be});\ e = 1, \ldots, E\} \tag{3}$$

that samples as well as possible all the probability distribution functions in Eq. (2) (see next section), with E being the number of samples.

To sample the probability distribution function $P(y)$, we select geophysical states y^e that cover all natural combinations and their correlations and by calculating x^e = RTM (y^e) with a radiative transfer model (i.e., physical inversion). We alternatively could obtain these relationships from a ''sufficiently large'' set of collocated and coincident values of x and y (i.e., empirical inversion). For sampling P_η, we need a priori information about the measurement noise characteristics; a physical noise model could be used, but if all we have is an estimate of the noise magnitude (as is the case here), we assume Gaussian distributed noise η that is not correlated among the measurements. To sample the first-guess variability with respect to state y [i.e., sampling $P(y^b|y]$, we use a first-guess dataset $\{y^{b^e};\ e = 1, \ldots, E\}$. This dataset can be a climatological dataset or a 6-h prediction (which would have better statistics of the errors but would add model dependencies). The balance between reliance on the first guess and the direct measurements is then made automatically and optimally by the neural network during the learning stage.

Once trained, the neural network g_W represents the inverse of the radiative transfer equation, statistically. The neural network model is then valid for all observations (i.e., global inversion), where iterative methods, such as variational assimilation, have to compute an estimator for each observation (i.e., local inversion).

b. The learning database

The learning database is limited to snow-covered areas. The snow flag is derived from the NOAA weekly snow maps. To constrain the problem (the problem is then better posed), we use the clear/cloudy flag information provided by the ISCCP dataset to train two neural networks: one for clear scenes (NN1) and one for cloudy scenes (NN2). This specialization of the neural networks facilitates the training of the neural network models. They both simultaneously retrieve the surface temperature Ts, the seven SSM/I surface emissivities e_f, and the integrated water vapor content WV. In addition to these parameters, NN2 retrieves the cloud LWP. Two sources of information are used for this purpose: 1) the seven SSM/I brightness temperatures, and 2) preexisting information of the state of the surface and atmospheric variables from ancillary datasets. A collection of SSM/I observations collocated and coincident with independent measurements of the parameters to be retrieved (Ts, e_f, WV, and LWP) is not available. However, with other estimates of Ts, e_f, WV, and LWP, the brightness temperatures can be simulated by a radiative transfer model, so the learning database uses these simulated brightness temperatures instead of observations. These radiative transfer results are obtained using selected values of Ts, WV, LWP, and e_f. To the extent that these datasets provide a proper distribution of the surface and atmospheric parameters, including their correlations, the neural network represents a global fit of the inverse radiative transfer model.

The atmospheric relative humidities and temperatures are taken from the NCEP reanalysis dataset (Kalnay et al. 1996), every 6 h at a spatial resolution of 2.5° in latitude and longitude. The columnar integrated WV is used as the first-guess a priori information, and the first-guess error is taken to be 0.4 times the first guess, similar to the WV error values obtained when using the error covariance of each humidity level as given by Eyre et al. (1993). In the ISCCP dataset, cloud and surface parameters are retrieved from visible (~0.6-μm wavelength) and infrared (~11-μm wavelength) radiances provided by the set of polar and geostationary meteorological satellites. In this study, the ISCCP dataset gives estimates of the cloud-top and surface skin temperatures. The pixel-level dataset (the ''DX'' dataset) is selected for its spatial sampling of about 30 km and time sampling of 3 h (Rossow et al. 1996). The error associated with the surface temperature is estimated to be 4 K (Rossow and Garder 1993). First-guess preexisting information for the microwave emissivities at each location is derived from the monthly mean emissivities previously estimated by Prigent et al. (1997, 1998, 2001a). The standard deviation of day-to-day variations of the retrieved emissivities within a month has been calculated for each channel and for each location and is used as estimates of first-guess errors for these quantities (see Fig. 2).

For more information on the a priori first-guess information and related background errors, see Aires et al. (2001).

TABLE 2. Global mean neural sensitivities (clear over snow). See section 4a for meaning of boldface.

	Ts	WV	e_{19V}	e_{19H}	e_{22V}	e_{37V}	e_{37H}	e_{85V}	e_{85H}
Ts	**0.23**	−0.07	−0.25	−0.16	−0.26	−0.20	−0.17	−0.16	−0.14
WV	−0.13	0.47	0.09	0.01	0.06	0.01	−0.08	−0.37	−0.54
Tb_{19V}	**0.26**	−0.28	**0.56**	−0.01	0.17	−0.17	−0.23	−0.02	0.13
Tb_{19H}	**0.10**	0.07	−0.05	**0.89**	−0.13	−0.22	0.00	−0.10	−0.19
Tb_{22V}	**0.10**	0.32	0.08	−0.16	**0.42**	−0.11	−0.23	−0.51	−0.63
Tb_{37V}	**0.08**	−0.02	−0.02	−0.13	0.06	**0.83**	0.10	0.09	−0.27
Tb_{37H}	**0.11**	−0.28	−0.18	0.03	−0.09	0.14	**0.94**	−0.02	0.40
Tb_{85V}	**0.13**	−0.08	−0.20	−0.11	−0.18	−0.01	−0.27	**1.20**	0.10
Tb_{85H}	**−0.01**	0.39	−0.02	−0.06	−0.07	−0.17	0.03	−0.12	**0.94**
e_{19V}	−0.13	0.02	0.16	0.11	0.17	0.13	0.11	0.11	0.11
e_{19H}	−0.12	0.00	0.15	0.11	0.15	0.12	0.12	0.12	0.13
e_{22V}	−0.12	0.01	0.15	0.10	0.16	0.12	0.11	0.11	0.12
e_{37V}	−0.09	0.01	0.10	0.08	0.11	0.10	0.09	0.10	0.11
e_{37H}	−0.06	−0.01	0.07	0.06	0.08	0.08	0.08	0.08	0.10
e_{85V}	−0.04	−0.02	0.05	0.04	0.06	0.05	0.06	0.08	0.09
e_{85H}	−0.03	−0.04	0.04	0.03	0.04	0.04	0.05	0.07	0.10

4. Results from the neural network inversions and discussion

a. Neural network sensitivities

The neural network technique enables an analytical and fast calculation of the neural Jacobians or neural sensitivities (Aires et al. 1999, 2001). These quantities provide a statistical estimation of the multivariate and nonlinear relationships among the input and output variables in terms of partial first derivatives. Table 2 gives the mean neural network sensitivities over snow for the clear-sky neural network. The neural Jacobians are normalized by the standard deviation (std) of the respective variables [$\partial x_k/\partial y_i \times \mathrm{std}(y_i)/\mathrm{std}(x_k)$] to enable comparison of the sensitivities between variables with different variation characteristics. They indicate the relative contribution of each input in the retrieval of each output. The sensitivities clearly show that the neural network manages to extract Ts and e_f with minimum correlation of errors. The sensitivities of the Ts retrieval are distributed over several of the inputs of the neural network, essentially the Tb_f and the Ts first-guess estimates, whereas the retrieval of each surface emissivity relies most heavily on the brightness temperature at the corresponding frequency (see the corresponding sensitivities in boldface in Table 2). Although, for each frequency, Tb_f is almost linearly related to Ts $\times$ e_f through the radiative transfer equation, simultaneous use of all the channel observations within the nonlinear neural network makes it possible to untangle the retrievals of Ts and e_f.

b. Theoretical accuracy

Figure 3 shows the normalized distributions of the retrieval errors calculated on the simulated dataset for Ts, WV, the emissivity at 19 GHz in horizontal polarization e_{19H}, and LWP as differences with the first-guess information (except for LWP that is compared with the ISCCP estimate that is not used as a first guess). The results are presented for three ranges of the emissivity at 85 GHz (horizontal polarization) and for clear and cloudy scenes, because different sensitivities to the retrieved parameters are expected depending on the surface and cloud characteristics. The distributions of the errors on the first guess are also indicated by dashed lines (except for LWP because no first-guess value was used). The surface types classified by monthly mean emissivities at 85 GHz in the horizontal polarization are roughly related to the snow characteristics, with the lower emissivities related to strong scattering in a dry snowpack due to the presence of large snow crystals. Cloudy scenes are divided into two groups according to their LWP estimated by ISCCP. For each histogram, the rms error is indicated along with the number of considered pixels (in parentheses). The results for each variable are briefly discussed.

The SSM/I observations have a good ability to measure the surface skin temperature with an averaged rms error of 1.52 K in clear areas and 1.95 K in cloudy cases. This rms error represents a large improvement over the first-guess rms of 4 K. The retrieval error is not affected much by the presence of clouds, and it decreases with increasing surface emissivity because of the increased contribution of the surface to the observed brightness temperatures.

Quantity WV is retrieved with a relative error of about 33% for clear situations and a relative error of about 26% in cloudy situations. This magnitude is also an improvement over the first-guess rms error of 40%. Contrary to the errors in Ts, the error in WV decreases with the surface emissivity: the contrast between the atmospheric and surface contribution increases with decreasing emissivity, making the atmospheric features easier to observe against a cold background. The retrieval errors are also slightly smaller in the presence of clouds, likely because of the larger WV amount in the cloudy regions.

For LWP, the theoretical rms error is 0.07 kg m^{-2} globally. As expected, the error is larger in areas of high

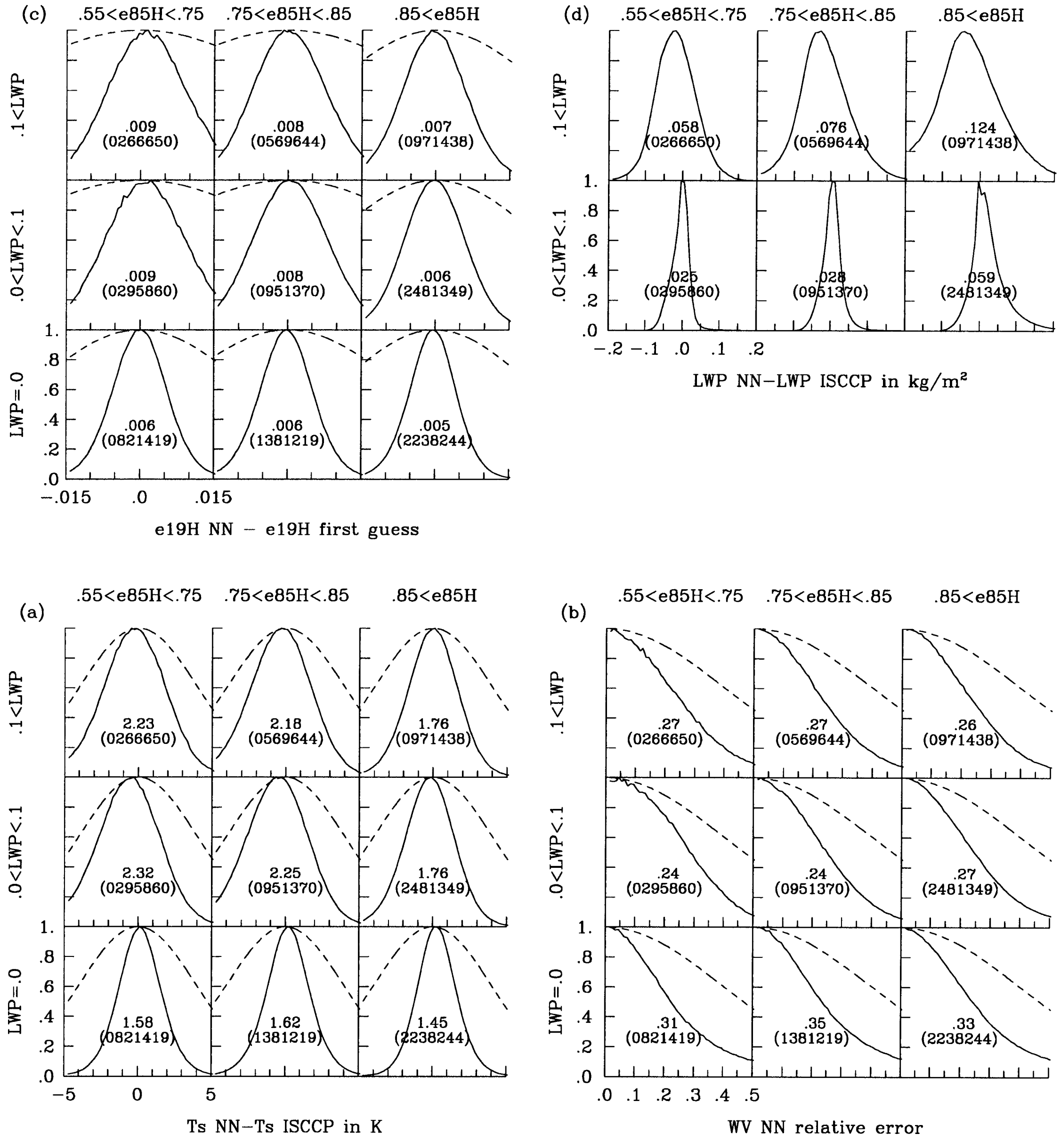

FIG. 3. For snow-covered areas, normalized distributions of the theoretical retrieval errors calculated on the simulated dataset for (a) Ts, (b) WV, (c) e_{19H}, and (d) LWP. Results are presented for three ranges of emissivities at 85 GHz (horizontal polarization) and for clear and cloudy scenes. The distributions of the errors on the first guess are also indicated (dash lines) except for LWP because no first-guess value is used. For each histogram, the rms error is indicated along with the number of considered pixels (in parentheses).

emissivities where the contrast between the land surface and the cloud is smaller. Even in areas of low emissivities ($0.55 < e_{85H} < 0.75$), the accuracy of the retrieval is not suitable for detection of the majority of clouds (Lin and Rossow 1994). As a consequence, the cloud flag from ISCCP is important to direct the retrieval toward the appropriate neural network. However, major cloud structures with large liquid water paths can still be detected.

The neural network technique retrieves snow surface emissivities with an rms error lower than 0.006 (0.010) globally for all channels, in clear conditions (cloudy conditions). This error is an improvement over the first-guess errors (see Fig. 2). The first guess provides the emissivity spectral relationship, and the retrieval exploits it to separate the emissivities from Ts. The possibility of retrieving several times daily the land surface emissivities with low rms errors would allow following the evolution of the snow characteristics as expressed in the microwave radiation. It can also improve the microwave retrieval of WV and temperature profiles over land: until recently a fixed emissivity was used for Microwave Sounder Unit retrievals over land, so there is a need for more accurate emissivity estimates (English 1999).

The neural networks have also been trained over continental ice. The theoretical results show characteristics that are very similar to the results over snow.

c. Evaluation of the results

The neural inversion method has been applied to a year of SSM/I *F10* and *F11* observations. In the operational mode, the neural network scheme is computationally very efficient. Inversion of new observations only involves simple and rapid calculations, two matrix products, and one pass through the logistic function of the neural network. Validation of the inversion results using independent measurements is challenging, because of the lack of coincident in situ measurements. Except for WV, which is routinely measured by radiosondes, the other retrieved variables are not part of the conventional in situ measurements. However, the retrieved products can be evaluated by checking that their space and time variations show the expected behavior with respect to other variables that are known to affect them.

1) Water vapor

The radiosonde measurements have been collected for 1992 and 1993. The WV estimates are compared with in situ measurements that are close in time (<1.5 h) and space (<20 km). The results are presented in Fig. 4 for clear (LWP = 0) and cloudy scenes (with cloud-top temperature Tc < 260 K and for warmer clouds). Here again, the results are separated by emissivity at 85 GHz. The rms of the difference is given along with the number of pixels (in parentheses). The results are very similar to the theoretical results and show a considerable improvement over the first-guess error (dashed lines in Fig. 4). For clear-sky conditions and for liquid water clouds (Tc > 260 K), the rms error decreases slightly with decreasing surface emissivities, as expected. Interaction of the radiation with ice particles within clouds is not taken into account in the learning database (cold clouds with Tc < 260 K), but the possibility of an underlying liquid cloud layer is allowed (Aires et al. 2001). As a consequence, in areas where large particles (precipitation) are likely to interfere with the signal, the retrieval can be in error.

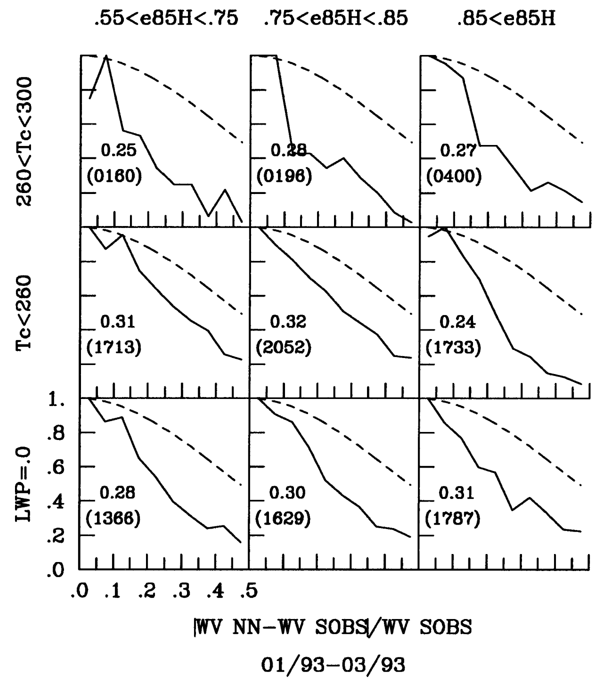

FIG. 4. Normalized histograms of the differences between WV estimates and WV radiosonde measurements, for clear (LWP = 0) and cloudy scenes (with cloud-top temperature Tc < 260 K and for warmer clouds). Results are separated by emissivity at 85 GHz. Rms of the difference is given along with the number of pixels (in parentheses). Distribution of the WV first-guess error is also shown (dashed lines).

2) Surface skin temperature

Surface skin temperature is not one of the conventionally measured variables, but near-surface air temperature Tair is routinely measured at surface weather stations every 3 h. Retrieved Ts and in situ measurements of Tair have been compared for all coincident observations. The variations of Ts − Tair with all the factors that could affect it have been examined. In general, the values of Ts − Tair exhibit the expected behavior, being larger for daytime than for nighttime, larger for clear days than for cloudy days, and larger for cloudy nights than for clear nights. However, the variations of Ts − Tair are made more complicated by the larger thermal inertia of snow (usually much larger than for snow-free soil) and its larger albedo; moreover, if temperatures are near freezing, then latent heat effects can influence the surface energy budget. All of these factors are expected to reduce the response of Ts to changes in solar heating. Indeed, not only are the day–night contrasts discussed earlier small, but the variations of Ts − Tair during the daytime (not shown) are small, with only a slight increase near midday. In contrast, the synoptic variations of Tair are very large in wintertime, suggesting that Ts is less variable than Tair. Figure 5 shows the mean values of Ts − Tair for each 1-K bin of Tair in three latitude ranges in North America. The behavior exhibited is as if there is an effective Teq at which Ts − Tair = 0. When Tair is above freezing over snow, Ts should remain near freezing until all the snow melts; thus, Ts − Tair will be negative. In general, when Tair changes rapidly, the thermal inertia of the snow should cause Ts to lag behind. As Fig. 5 shows, the changeover from negative to positive occurs at temperatures well below freezing, decreasing with increasing latitude, as would be expected for a decreasing solar input to the energy balance. We find that Teq is close to the average Ts over the whole time period for each latitude zone, so it appears that when Tair increases or

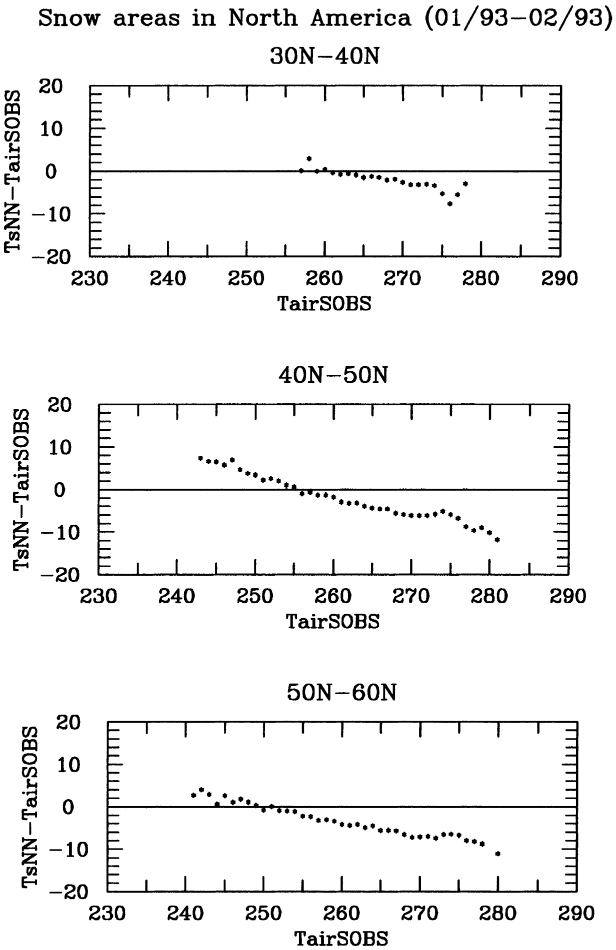

FIG. 5. Mean difference between Ts and Tair for each 1-K bin of Tair for three latitude ranges in North America. Comparison includes all coincident observations, clear and cloudy, night and day.

decreases above the average value of Ts, the values of Ts remain closer to Teq, producing negative Ts − Tair when Tair > Teq and positive Ts − Tair when Tair < Teq. This behavior is found even if we limit the results to clear scenes and use only the ISCCP values of Ts.

3) SURFACE EFFECTIVE EMISSIVITIES

The snow emissivity is estimated for the seven SSM/I channels for both clear and cloudy scenes. Evaluation of this product is a challenging task, given the absence of any large-scale study of this parameter. However, one can check that 1) temporal and spatial variations in surface emissivities can be reasonably interpreted in terms of variations in snowpack properties or other surface characteristics and 2), for a given area, the expected frequency and polarization dependences are observed among the seven channel emissivities.

Figure 6 shows the variation of the monthly mean retrieved emissivities (clear and cloudy) at 19, 37, and 85 GHz (horizontal polarization) versus monthly mean

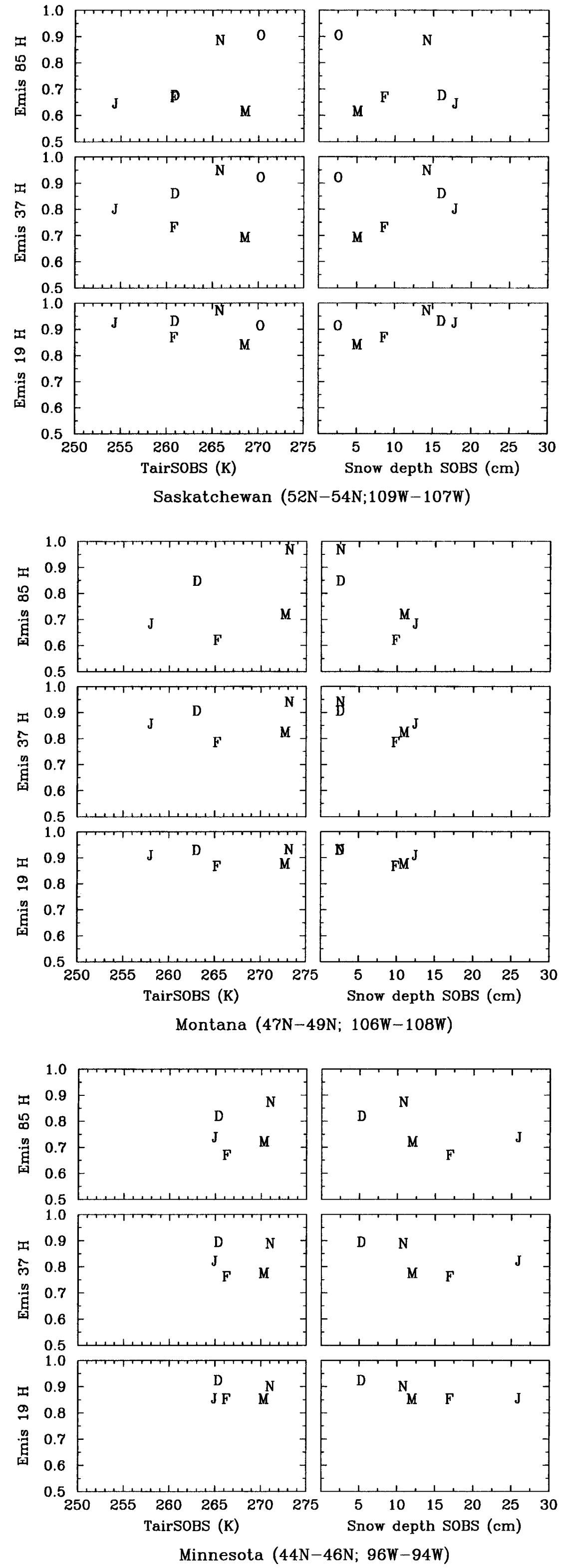

FIG. 6. Monthly mean retrieved emissivities at 19, 37, and 85 GHz (horizontal polarization) monthly mean in situ surface air temperature and snow depths for three locations in North America. Monthly mean values are indicated by the first letter of each month.

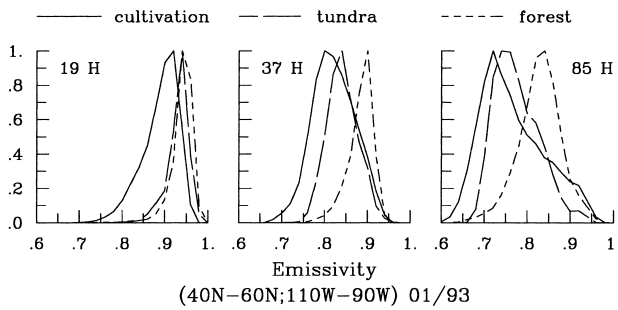

FIG. 7. Normalized histograms of the retrieved emissivities at 19, 37, and 85 GHz (horizontal polarization) for three types of vegetation in North America (40°–60°N, 110°–90°W) in Jan 1993.

in situ surface air temperatures and snow depths for three locations in North America. The high-frequency emissivities, especially at 85 GHz, decrease with air temperature during the first part of the winter, but, once the minimum air temperature is reached and the temperature starts to increase (in February in the three cases shown), the emissivities monotically decrease before increasing again just at the end of the snow season. This hysteresis cycle can be explained by increasing grain sizes through different processes during the winter until snow melts (Sturm and Benson 1997). This interpretation of the snow history is consistent with the observed frequency dependence: The amplitude of this cycle increases with frequency because of a larger contribution of the scattering process within the snowpack at higher frequency. No clear dependence is observed between the emissivities and snow depth. Other locations were checked and gave similar responses.

The retrieved emissivities also show significant and expected variations with the vegetation cover. In central North America, a strong and clear vegetation gradient is observed going northward from cultivated areas up to approximately 50° to evergreen needle–leaved forests up to about 60° to arctic tundra (Matthews 1983). Normalized histograms of the retrieved emissivities at 19, 37, and 85 GHz (horizontal polarization) are presented in Fig. 7 for these three types of vegetation in central North America (40°–60°N, 110°–90°W) in January of 1993, using the Matthews vegetation classification. The sensitivity of the snow emissivity to vegetation cover increases with frequency, with the 19-GHz response varying only weakly. At 37 and 85 GHz, the presence of dense evergreen vegetation above the snow-covered ground increases the emissivity, as expected: Emissivity histograms of forested areas are well separated from the other two (cultivation and tundra) that correspond to low-density vegetation cover, especially during wintertime.

It is difficult to retrieve snow depth from microwave emissivities at these frequencies on a global basis, given the limited correlation observed between the two variables, even when the effects of temperature have been removed as in our results. However, the snow emissivities exhibit systematic variations with other snow and surface parameters that are worth exploring (e.g., snow history or vegetation cover). Combining satellite observations at different frequencies and observational mode (passive and active) will be examined, in order to benefit from the synergy between the various measurements. Such an approach has already proved productive for vegetation analysis (Prigent et al. 2001a) and for the estimation of inundation extent and seasonality (Prigent et al. 2001b).

5. Concluding remarks

From SSM/I observations between 19 and 85 GHz, atmospheric water vapor, cloud liquid water, surface temperature, and surface emissivities have been retrieved over snow using a neural network inversion scheme that includes first-guess information. A learning database to train the neural network is derived from a global collection of coincident surface and atmospheric parameters, extracted from the NCEP reanalysis, from the ISCCP data, and from microwave emissivity atlases previously calculated. In the operational mode, inversion of new observations with the neural network only involves simple and rapid calculations, which is a very important asset when processing large volumes of global observations.

The surface and atmospheric parameters can be retrieved, despite the large space and time variabilities of the microwave snow response. Most important, the effects of varying surface temperature can be isolated to determine the variations of snow emissivities better. Evaluation of the estimated variables using independent measurements has been completed for integrated water vapor. The other variables are not routinely measured, and so validation is a challenging task and cannot be performed quantitatively.

Water vapor is retrieved with a theoretical rms error of approximately 30%. It has been validated against radiosonde measurements, and the resulting relative errors are of the same order. In polar regions where in situ measurements are limited, this analysis is an attractive alternative. Recent studies by Miao (1998) and Wang et al. (2001) also showed promising water vapor estimates over boreal regions from observations at higher frequencies (between 150 and 190 GHz). Comparison of the two approaches could lead to a combined use of the whole frequency range from 19 to 190 GHz. In addition, Haggerty et al. (2002) showed the potential of airborne microwave measurements for liquid water retrieval over sea ice.

The theoretical rms error of the surface temperature retrieval (i.e., using simulated dataset) is 1.52 K in clear-sky conditions and 1.95 K in cloudy scenes. Although the surface air temperature is available from in situ measurements, the surface skin temperature is not, and differences between surface skin and surface air temperatures are a complex function of the surface and atmospheric characteristics and solar flux, making very difficult any real validation of the Ts product. Microwave land surface temperature retrieval in cloudy areas is a promising complement to the infrared estimates in clear areas. By combining IR and microwave measurements, a complete (clear and cloudy) time record of land surface temperatures can now be produced. Energy and water exchanges at the land–atmosphere interface are controlled, in part, by the difference of air and skin temperatures. Measurements of the air and skin temperatures, with time resolution that is high enough to resolve the diurnal cycle under all synoptic conditions and that covers a long enough period to examine how different seasonal and interannual conditions affect them, are required to study the energy and water exchange processes at the land–atmosphere interface.

The surface emissivities are retrieved with an accuracy of 0.010 even in cloudy conditions. The sensitivity of the microwave emissivities to snow depth is questioned. However, microwave emissivities show interesting variations with other snow characteristics, especially at higher frequencies. Simultaneous analysis of retrieved microwave emissivities, active microwave observations (scatterometer and altimeter on board European Remote Sensing Satellites) and visible and near-infrared observations (Advanced Very High Resolution Radiometer) is now under way to assess the sensitivity of the various observations to the snow characteristics. The various observations will be merged to benefit from their complementarity and, possibly, to extract snow physical properties from these satellite measurements.

Long time series (10 yr) of the retrieved products are now being calculated. The interannual variability of the snow characteristics will be analyzed, along with the surface temperature and the other atmospheric parameters, for their implications in climate and hydrological studies.

Acknowledgments. The Global Hydrology Data Center (NASA Marshall Space Flight Center) provided the SSM/I dataset. NCEP reanalysis data are provided by the NOAA–CIRES Climate Diagnostics Center, Boulder, Colorado, from the Internet at http://www.cdc.noaa.gov/. The authors thank Cindy Pearl and Ralph Karow from GISS, New York, for their help in processing the data. They are grateful to Nelly Mognard from CNES, France, for fruitful discussions. They also thank three anonymous reviewers for a careful reading of the manuscript.

REFERENCES

Abdalati, W., and K. Steffen, 1997: Snowmelt on the Greenland ice sheet as derived from passive microwave satellite data. *J. Climate,* **10,** 165–175.

Aires, F., M. Schmitt, N. A. Scott, and A. Chédin, 1999: The weight smoothing regularization for Jacobian stabilization. *IEEE Trans. Neural Networks,* **10,** 1502–1510.

——, C. Prigent, W. B. Rossow, and M. Rothstein, 2001: A new neural network approach including first guess for retrieval of atmospheric water vapor, cloud liquid water path, surface temperature and emissivities over land from satellite microwave observations. *J. Geophys. Res.,* **106,** 14 887–14 907.

Chang, A. T. C., P. Gloersen, T. Schmugge, T. T. Wilheit, and H. J. Zwally, 1976: Microwave emission from snow and glacier. *J. Glaciol.,* **16,** 23–39.

——, J. L. Foster, and D. K. Hall, 1987: *Nimbus-7* SSMR derived global snow cover parameters. *Ann. Glaciol.,* **9,** 39–44.

English, S. J., 1999: Estimation of temperature and humidity profile information from microwave radiances over different surface types. *J. Appl. Meteor.,* **38,** 1526–1541.

Eyre, J. R., G. A. Kelly, A. P. MacNelly, E. Anderson, and A. Persson, 1993: Assimilation of TOVS radiance information through one-dimensional variational analysis. *Quart. J. Roy. Meteor. Soc.,* **119,** 1427–1463.

Foster, J. L., A. T. C. Chang, R. J. Gurney, F. Hewer, and R. Essery, 1994: Snow cover and snow mass estimates from remote sensing, climatology, and the United Kingdom Meteorological Office General Circulation Model. *ESA/NASA International Workshop,* B. J. Choudhury et al., Eds., VSP, 55–76.

——, and Coauthors, 1996a: Snow-mass intercomparisons in the boreal forests from general circulation models and remotely sensed data sets. *Polar Rec.,* **32,** 199–208.

——, and Coauthors, 1996b: Snow cover and snow mass intercomparisons of general circulation models and remotely sensed datasets. *J. Climate,* **9,** 409–426.

Grody, N. C., and A. N. Basist, 1996: Global identification of snowcover using SSM/I measurements. *IEEE Trans. Geosci. Remote Sens.,* **34,** 237–249.

Haggerty, J. A., J. A. Curry, and G. Liu, 2002: Potential for estimating cloud liquid water path over sea ice from airborne passive microwave measurements. *J. Geophys. Res.,* **107,** 2–13.

Hall, D. K., M. Sturm, C. S. Benson, A. T. C. Chang, J. L. Foster, H. Garbeil, and E. Chacho, 1991: Passive microwave remote and in situ measurements of Arctic and subarctic snow covers in Alaska. *Remote Sens. Environ.,* **38,** 161–172.

Hewison, T. J., and S. J. English, 1999: Airborne retrievals of snow and ice surface emissivity at millimeter wavelengths. *IEEE Trans. Geosci. Remote Sens.,* **37,** 1871–1887.

Josberger, E. G., and N. M. Mognard, 2002: A passive microwave snow depth algorithm with a proxy for snow metamorphism. *Hydrol. J.,* in press.

Kalnay, E., and Coauthors, 1996: The NCEP/NCAR 40-Year Reanalysis Project. *Bull. Amer. Meteor. Soc.,* **77,** 437–471.

Kunzi, K. F., S. Patil, and H. Rott, 1982: Snow-cover parameter retrieved from *Nimbus-7* Scanning Multichannel Microwave Radiometer (SMMR) data. *IEEE Trans. Geosci. Remote Sens.,* **4,** 452–467.

Kurvonen, L., and M. Hallikainen, 1997: Influence of land-cover category of brightness temperature of snow. *IEEE Trans. Geosci. Remote Sens.,* **35,** 367–377.

Lin, B., and W. B. Rossow, 1994: Observations of cloud liquid water path over oceans: Optical and microwave remote sensing methods. *J. Geophys. Res.,* **99,** 20 907–20 927.

Matthews, E., 1983: Global vegetation and land use: New high-resolution data bases for climate studies. *J. Climate Appl. Meteor.,* **22,** 474–487.

Matzler, C., 1994: Passive microwave signatures of landscapes in winter. *Meteor. Atmos. Phys.,* **54,** 241–260.

Miao, J., 1998: Retrieval of atmospheric water vapor content in polar regions using spaceborne microwave radiometry. Ph.D. dissertation, University of Bremen, Bremen, Germany, 109 pp.

Noll, J., J. P. V. Poires Baptista, M. Borgeaud, and A. Rognes, 1994: Multitemporal aspects in snow retrieval using spaceborne radiometers. *Specialist Meeting on Microwave Radiometry and Remote Sensing Application,* VSP, 211–214.

Prigent, C., W. B. Rossow, and E. Matthews, 1997: Microwave land surface emissivities estimated from SSM/I observations. *J. Geophys. Res.,* **102,** 21 867–21 890.

——, ——, and ——, 1998: Global maps of microwave land surface emissivities: Potential for land surface characterization. *Radio Sci.,* **33,** 745–751.

——, F. Aires, W. B. Rossow, and E. Matthews, 2001a: Joint characterization of the vegetation by satellite observations from visible to microwave wavelengths: A sensitivity analysis. *J. Geophys. Res.,* **106,** 20 665–20 685.

——, E. Matthews, F. Aires, and W. B. Rossow, 2001b: Remote sensing of global wetland dynamics with multiple satellite data sets. *Geophys. Res. Lett.,* **28,** 4631–4634.

Pulliainen, J., and M. Hallikainen, 2001: Retrieval of regional snow water equivalent from space-borne passive microwave observations. *Remote Sens. Environ.,* **75,** 76–85.

Robinson, D. A., and T. E. Spies, 1994: Monitoring snow cover on the Tibetan Plateau using passive microwave satellite data. *ESA/NASA International Workshop,* B. J. Choudhury et al., Eds., VSP, 285–294.

Rossow, W. B., and R. A. Schiffer, 1991: ISCCP cloud data products. *Bull. Amer. Meteor. Soc.,* **72,** 2–20.

——, and L. C. Garder, 1993: Validation of ISCCP cloud detections. *J. Climate,* **6,** 2370–2393.

——, and R. A. Schiffer, 1999: Advances in understanding clouds from ISCCP. *Bull. Amer. Meteor. Soc.,* **80,** 2261–2287.

——, A. W. Walker, D. E. Beuschel, and M. D. Roiter, 1996: International Satellite Cloud Climatology Project (ISCCP): Document on new cloud datasets. NASA Goddard Institute for Space Studies, 115 pp.

Rott, H., and T. Nagler, 1994: Intercomparison of snow retrieval algorithms by means of spaceborne microwave radiometry. *ESA/NASA International Workshop,* B. J. Choudhury et al., Eds., VSP, 227–243.

Rumelhart, D. E., G. E. Hinton, and R. J. Williams, 1986: Learning internal representations by error propagation. *Parallel Distributed Processing: Explorations in the Microstructure of Cognition.* Vol. I, *Foundations,* D. E. Rumelhart, J. L. McClelland, and the PDP Research Group, Eds., MIT Press. 318–362.

Schanda, E., C. Matzler, and K. Kunzi, 1983: Microwave remote sensing of snow cover. *Int. J. Remote Sens.,* **4,** 149–158.

Singh, P. R., and T. Y. Gan, 2000: Retrieval of snow water equivalent using passive microwave brightness temperature data. *Remote Sens. Environ.,* **74,** 275–286.

Sturm, M., and C. S. Benson, 1997: Vapor transport, grain growth and depth-hoar development in the subarctic snow. *J. Glaciol.,* **43,** 42–58.

——, J. Holmgren, and G. E. Liston, 1995: A seasonal snow cover classification system for local to global applications. *J. Climate,* **8,** 1261–1283.

Tsang, L., 1992: Dense media radiative transfer theory for dense discrete random media with spherical particles of multiple sizes and permittivities. *Progress in Electromagnetics Research,* A. Priou, Ed., Vol. 6, Elsevier, 181–230.

Wang, J. R., P. E. Racette, and M. E. Triesky, 2001: Retrieval of precipitable water vapor by the millimeter-wave imaging radiometer in the Arctic region during FIRE-ACE. *IEEE Trans. Geosci. Remote Sens.,* **39,** 595–605.